XRD analysis of nanocrystalline anatase powders prepared by various chemical routes: correlations between micro-structure and crystal structure parameters

Z. Matěj[a*], L. Matějová[b], and R. Kužel[a]

* Corresponding author. E-mail: matej@karlov.mff.cuni.cz

[a] *Department of Condensed Matter Physics, Faculty of Mathematics and Physics, Charles University in Prague, Ke Karlovu 5, 121 16 Praha 2, Czech Republic*

[b] *Department of Catalysis and Reaction Engineering, Institute of Chemical Process Fundamentals of the ASCR, v.v.i., Rozvojová 135, 165 02 Praha 6, Czech Republic*

Nanocrystalline anatase powders synthesised by various chemical processes as super/subcritical fluid extraction, sol-gel technique and hydrolysis of titanium alkoxides in hydrogen peroxide were studied by X-ray diffraction (XRD) whole profile modelling method (WPPM) in order to reveal correlations between structural and micro-structural parameters as well as sample treatment conditions. Anisotropy of the diffraction line broadening due to truncated bipyramidal shape of anatase crystals was discussed. The *hkl*-anisotropy can be very strong but also almost negligible in dependence on relative ratio of the crystallite dimensions. The latter was the case for the studied samples. The size of synthesised anatase nanoparticles was within the range 3–25 nm. The theoretical total surface area of crystallites calculated from XRD was in a good correlation with the surface area measured by the nitrogen physisorption up to the temperature 400–450 °C, when the particles started to agglomerate. At atomic scale a unit cell volume contraction with decreasing crystallite size and a significant deficiency in the Ti-site occupancy was observed. Both effects were attributed to the presence of Ti-vacancies and a linear coefficient between the relative cell volume contraction and the fraction of Ti-vacancies was estimated to (–0.017±0.003).

Key words: XRD, anatase, crystallite size, lattice parameters, vacancies, anisotropy

I. INTRODUCTION

Synthesis of nanocrystalline porous metal oxides (namely TiO_2) has been an important topic of scientific efforts for many decades. Excellent photochemical activity of titania (Hashimoto *et al.*, 2005; Fujishima and Zhang, 2006) and other photo-induced phenomena (Sakai *et al.*, 2003; Mills *et al.*, 2003; Wang *et al.*, 2001) are basis of novel applications of this apparently simple material. Usually the objective is preparation of crystalline material of high chemical purity, phase composition, with a given particle size as well as a reasonable size dispersion and particles morphology. Diffraction methods assist in this aim as analytical tools. In last years, there were many structural studies revealing interesting phenomena of nanocrystalline TiO_2. It is well known (Hanaor and Sorrell, 2011) that rutile is the stable TiO_2 phase at the ambient conditions, whereas bulk anatase and brookite are considered to be metastable. Zhang and Banfield (1998) found that this is different for nanocrystallites, as anatase and brookite are thermodynamically more stable than nanocrystalline rutile. Arlt *et al.* (2000) reported about other TiO_2 polymorphs. Zhang *et al.* (2008) studied also amorphous TiO_2 and its transformation to nanocrystalline anatase by using pair-distribution function, Monte Carlo simulations and X-ray absorption spectroscopy. X-ray diffraction (XRD) analysis of residual stresses in thin TiO_2 films and elastic anisotropy of anatase were described in (Borgese *et al.*, 2011; Bontempi *et al.*, 2010; Kužel *et al.*, 2010; Matěj *et al.*, 2011b). Size dependent elasticity of nanocrystalline titania was studied in high pressure synchrotron experiment by Chen *et al.* (2009). Kinetics of crystallisation of anatase nanoparticles was investigated in (Zhang and Banfield, 2002; Li *et al.*, 2005; Jensen *et al.*, 2010; Kužel *et al.*, 2010). Dislocations in nanocrystalline anatase were characterised by the whole powder pattern modelling method (WPPM) (Scardi and Leoni, 2002) in Spadavecchia *et al.* (2010). The Debye function method was used for analysis of size and shape of TiO_2 nanocrystals in (Cernuto *et al.*, 2011). Yang *et al.*, (2008) and Li and Liu (2011) observed anatase particles of a truncated bipyramidal shape and discussed the shape effects on the material properties. Transmission electron microscopy (TEM), nitrogen adsorption, mercury porosimetry and XRD analysis using the Williamson-Hall (WH) plot method were applied for particle size determination by Weibel *et al.* (2005). Different methods of line profile analysis (LPA) were compared on a set of sol-gel TiO_2 powders in a thorough study of Vives and Meunier (2009).

https://doi.org/10.1017/S0885715613001061 Published online by Cambridge University Press

In recent years the present authors have developed different methods of synthesis of nanocrystalline anatase mainly for photo-catalytic and photo-electro-chemical-sensing applications. A facile method of synthesis of nanocrystalline TiO_2 – (i) Low-temperature hydrolysis of titanium alkoxide in hydrogen peroxide solution followed by calcination at temperature 300 °C and higher – was presented in (Matějová *et al.*, 2012a). Anatase powders prepared by (ii) calcination of sol-gel titania organogels were used as reference samples for histogram-like crystallites size distribution (CSD) determination from XRD data in (Matěj *et al.*, 2011a). At last, instead of the calcination at elevated temperatures (iii) subcritical fluid extractions techniques were utilised to obtain crystalline titania in (Matějová *et al.*, 2010; Matějová *et al.*, 2012b). The methods differ in various manners. The most pronounced advantage of the first one is that the organogel preparation is omitted and the synthesis yield is much higher. Details about syntheses as well as discussions concerning mainly effects of individual technological steps on material microstructure, porous structure and chemical purity were reported in the mentioned papers, but detailed information about crystal structure parameters and a comparative study of these parameters among different series of samples are missing there. Samples prepared by all these routes were analysed by the WPPM method giving rich information from the atomic (atom positions) to micrometer scale (e.g. crystallite size). Detailed results are presented here and compared with the literature in order to reveal correlations within the micro-structural parameters as well as sample treatment conditions and the material properties.

II. EXPERIMENTAL

A. Samples preparation

Three series of samples prepared by different chemical routes are studied in this work. Sample nomenclature is defined and essential technological parameters are listed in Table I. Details of samples preparation can be found in literature (references, Table I) and are described only briefly here.

1. Samples nBUT(300—450), ISOP400 and ISOP400/10 were prepared by low-temperature hydrolysis of titanium (IV) alkoxides in hydrogen peroxide solution followed by calcination of the amorphous titania peroxo-product at temperature 300 °C and higher. Samples labelled as nBUT were prepared from n-butoxide, samples named as ISOP from isopropoxide. All samples were calcined for 4 hours with an exception of ISOP-400/10, which was calcined for 10 hours. [see (Matějová *et al.*, 2012a)]

https://doi.org/10.1017/S0885715613001061 Published online by Cambridge University Press

2. Samples REF-400 and REF-550 were prepared by calcination of rigid titania organogels synthesised by a sol-gel process. Titanium (IV) isopropoxide was added drop by drop into the formed reverse micellar environment of cyclohexane, nonionic surfactant Triton X-100 and water. After 24 hours ageing on the air the prepared sol converted into the rigid organogel. Organogel was calcined in a muffle furnace at 400 °C and 550 °C respectively. [see (Matěj *et al.*, 2011a)]

3. Sample ISOP-SubWE/PFE was prepared from a surfactant-mediated titania organogel by a combination of subcritical water extraction and pressurised alcohol extraction. The rigid organogel was prepared by a similar procedure as in the previous case; with a difference the Triton X-114 surfactant was used. The gel was than extracted at temperature 200 °C and pressure 10 MPa by subcritical water (SubWE) and pressurised fluid (PFE), using methanol. [see (Matějová *et al.*, 2010)]

TABLE I. List of studied TiO_2 nanocrystalline powder samples.

ID	alkoxide	method	Temp./Time	ref.
nBUT-300	n-butox.	hydrolysis/ calcination	300 °C/4h	(Matějová *et al.*, 2012a)
nBUT-330			330 °C/4h	
nBUT-380			380 °C/4h	
nBUT-450			450 °C/4h	
ISOP-400	isopropox.		400 °C/4h	
ISOP-400/10			400 °C/10h	
REF-400		gel/calcination	400 °C/4h	(Matěj *et al.*, 2011a)
REF-550			550 °C/12h	
ISOP-SubWE/PFE		gel/extraction	200 °C/10 MPa	(Matějová *et al.*, 2010; Matějová *et al.*, 2012b)

Finally all the synthesised samples had a form of white powders.

B. XRD measurements

Specimens were measured using a PANalytical MPD X'Pert Pro diffractometer in the Bragg-Brentano geometry, with Ni-filtered Cu *Kα*-radiation, variable divergence and anti-scatter slits. The axial divergence was controlled by 0.04 rad Soller slits. The diffracted intensity was

https://doi.org/10.1017/S0885715613001061 Published online by Cambridge University Press

recorded by a PIXCel position-sensitive detector. The NIST LaB_6 standard was measured in the same experimental arrangement to get corrections on instrumental broadening effects.

III.XRD ANALYSIS

XRD data were analysed using the MSTRUCT software (Matěj and Kužel, 2009; Matěj *et al.*, 2010) implementing the WPPM method (Scardi and Leoni, 2002). The MSTRUCT is based on a free crystallographic library ObjCryst/FOX (Favre-Nicolin and Černý, 2002). The WPPM method combines the Fourier modelling of diffraction line profiles (Scardi and Leoni, 2001) with the Rietveld refinement of crystal structure parameters.

A. Crystal structure model

Anatase was major crystalline phase present in the samples. Hence a choice of its structural model was crucial to achieve a good pattern fit. Crystal structure parameters of sol-gel synthesised nanocrystalline anatase reported by Djerdj and Tonejc (2006) – ICSD#154603 (FIZ Karlsruhe, 2012), space group $I4_1/amd$ (141) with origin at centre (2/*m*) – were used as the starting model.

During typical data fitting procedure the lattice parameters of anatase, *z*-fractional coordinate of the oxygen atom at the 8*e* site, isotropic Debye-Waller (DW) factors B_{iso} of both scattering atoms and the occupancy of the titanium 4*b* site were refined. At the beginning it was supposed the oxygen site did not need to be fully occupied due to the presence of oxygen vacancies. However, as the refinement of the oxygen occupancy did not improve the fits and it rather destabilised the procedure, the oxygen occupancy was fixed to unity.

B. Microstructure models

The aim of this work is a cross-series comparison of the synthesised TiO_2 samples; hence a basic simplified microstructural model, which was used for XRD analysis of all the samples in (Matějová *et al.*, 2012a; Matěj *et al.*, 2011a; Matějová *et al.*, 2010), is also applied here. The crystallites size broadening was described by the model of spherical particles with diameter distributed according to the log-normal distribution [e.g. (Langford *et al.*, 2000; Scardi and Leoni, 2001; Scardi and Leoni, 2002)]. The model has two parameters: *M* is the median and σ^* is the multiplicative standard deviation (Limpert *et al.*, 2001) of the crystallites size distribution (CSD). Diffraction line broadening due to lattice microstrains was in most cases here a minor

https://doi.org/10.1017/S0885715613001061 Published online by Cambridge University Press

and weak effect; hence a simple *hkl*-isotropic phenomenological model (Matěj and Kužel, 2009; Matěj *et al.*, 2010) was used. The model has two parameters: microstrain *e* (%), characterising the defects effect strength, and parameter η characterising Gauss-Lorentz character of the pseudo-Voigt function used for modelling the diffraction profiles from defect induced broadening.

For both broadening effects above more advanced models, which can also describe *hkl*-anisotropic diffraction line broadening, are available in Rietveld software – as e.g. phenomenological models of Popa (1998) and Stephens (1999). Physically more relevant models often utilise the Fourier modelling approach. Such model of dislocation induced broadening in materials with lower than cubic lattice symmetry was introduced by Leoni *et al.* (2007). The size-broadening model, published recently (Leonardi *et al.*, 2012), accounts generally for the anisotropic crystallites shape. Validity of all these models and the WPPM is limited to particles larger than few nanometres. Contrary the Debye formula method is computationally demanding for particles of size over few tens of nanometres. Beyerlein *et al.* (2011) have shown that by including some corrections the WPPM is sufficiently accurate also for crystallites as small as 2 nm. Hence finally, it was assumed, that the use of WPPM for the problem under study here is justified. The appropriateness of the simplified models above for the studied materials is furthermore demonstrated in the next section.

IV. RESULTS

Refined parameters are listed in Table II. The samples are sorted according to the anatase crystallites size. The character as well as the content of minor crystalline phase, if any, are also noted in the Table II. It is evident that there is nonnegligible amount of brookite (~ 23 wt.%) in the ISOP-SubWE/PFE sample with the smallest anatase crystallites size (M ~ 3.5 nm) and a small amount of rutile (~ 7 wt.%) in the REF-550 sample with the largest anatase crystallites (M ~ 21 nm), which was treated at the highest annealing temperature (550 °C). This is related to the thermodynamical stability of different TiO_2 nanocrystalline phases and it agrees with the theory of Zhang and Banfield (1998). Following discussion is related solely to the anatase phase, which is the major crystalline phase in all the samples. Quality of a typical pattern fit is depicted in Figure 1.

https://doi.org/10.1017/S0885715613001061 Published online by Cambridge University Press

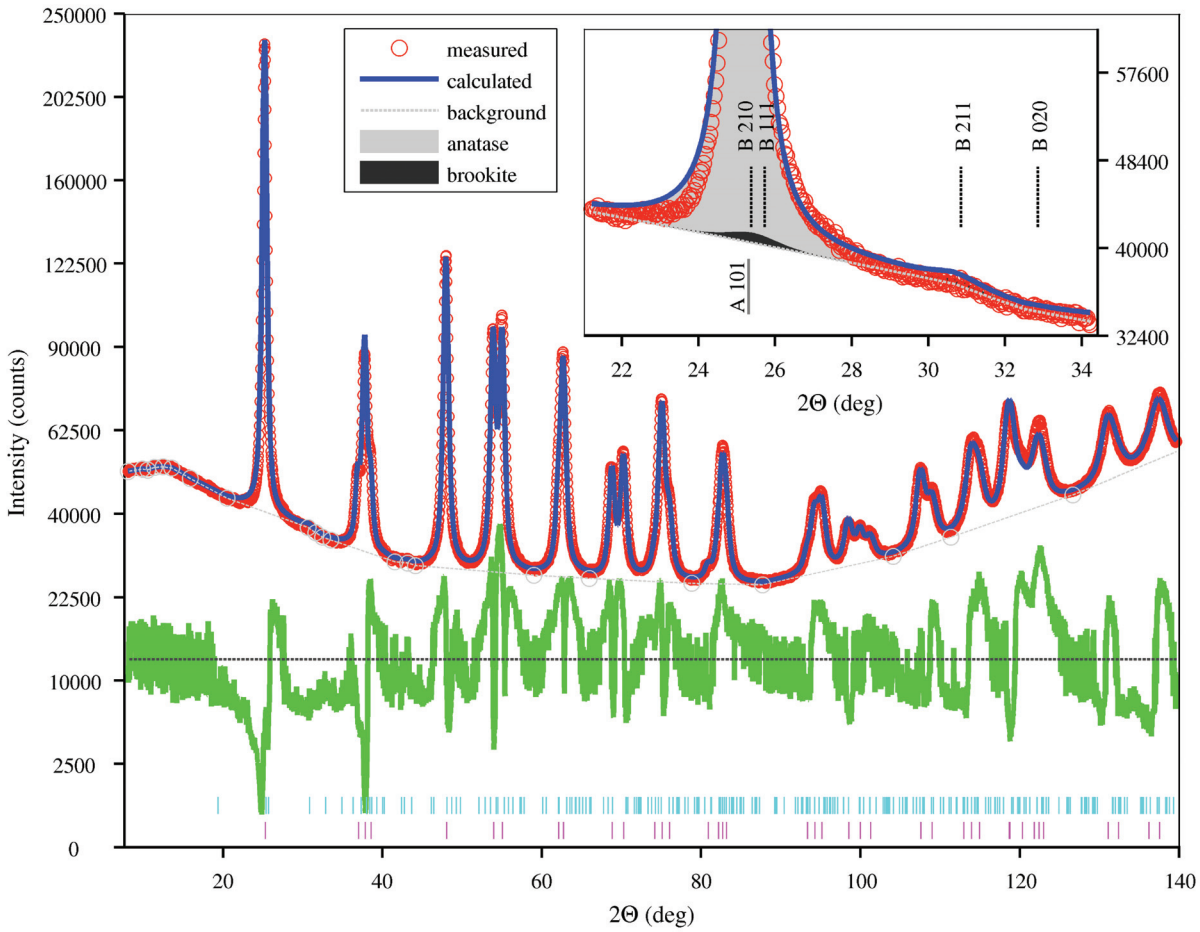

Figure 1. (Color online) Pattern fit of the nBUT-450 sample. Small ticks at the bottom mark the anatase reflections, whereas the ticks above indicate reflections of the minor brookite phase.

https://doi.org/10.1017/S0885715613001061 Published online by Cambridge University Press

TABLE II. Refined structural and microstructural parameters of the studied TiO_2 nanocrystalline powder samples. Values marked by a star superscript (*) were not refined but set to a fixed value.

M ... median of anatase CSD,

σ^* ... multiplicative standard deviation of anatase CSD,

a, *c* ... anatase lattice parameters,

B(Ti), *B*(O) ... isotropic Debye-Waller factors of Ti and O,

z(O) ... fractional *z*-coordinate of the Ti-atom,

Occ(Ti) ... anatase Ti-occupancy,

e ... microstrain in anatase crystallites,

η ... shape parameter of the microstrain effect in anatase (0 ... Gaussian, 1 ... Lorentzian),

minor phase ... identified in the pattern (B ... brookite, R ... rutile),

$x_{anatase}$ ... weight fraction of anatase,

M_m ... median of minor phase CSD (assumed the log-normal distrib. with $\sigma_m^*=1.35^*$).

sample ID	***M*** **(nm)**	$\boldsymbol{\sigma^*}$	*a* (Å)	*c* (Å)	*B*(Ti) (Å^2)	*B*(O) (Å^2)	*z*(O)	*Occ*(Ti)	***e*** **(%)**	η	**minor phase**	$\boldsymbol{x_{anatase}}$ **(wt.%)**	M_m (nm)
ISOP-SubWE/PFE	**3.2**(3)	**1.49**(4)	3.789(1)	9.465(4)	2.8(1)	9.7(3)	0.170(1)	0.72(2)	**0.8**(1)	0.0(1)	**B**	**77**(1)	3.7(2)
nBUT-300	**4.5**(2)	**1.46**(1)	3.7881(4)	9.483(1)	0.43(4)	2.5(1)	0.1651(3)	0.87(1)	**0.2**(2)	0.7(8)	**B**	**93.2**(4)	5*
REF-400	**6.2**(1)	**1.473**(6)	3.7868(1)	9.5033(3)	0.55(1)	1.94(3)	0.1664(1)	0.95(1)	**0.19**(8)	0.9(5)	**R**	**99.58**(3)	32*
nBUT-330	**6.4**(3)	**1.45**(2)	3.7872(3)	9.482(1)	0.33(3)	2.6(1)	0.1671(3)	0.90(1)	**0.3**(2)	1.0(7)	**B**	**93.1**(5)	5*
nBUT-380	**8.6**(2)	**1.39**(1)	3.7873(2)	9.4931(5)	0.01(2)	1.10(6)	0.1665(2)	0.95(1)	**0.33**(4)	0.9(1)	**B**	**95.4**(3)	5*
nBUT-450	**10.3**(4)	**1.51**(2)	3.7872(1)	9.5060(3)	0.00(2)	0.35(3)	0.1658(1)	1.00(1)	**0.23**(3)	0.7(1)	**B**	**98.1**(4)	5*
ISOP-400/10	**13**(1)	**1.79**(5)	3.78691(5)	9.5070(4)	0.14(1)	0.50(2)	0.1666(1)	1.00(1)	**0.345**(4)	0.59(2)	**R**	**98.7**(5)	8*
ISOP-400	**13**(2)	**1.80**(5)	3.78647(5)	9.5078(2)	0.00(1)	0.36(2)	0.1668(1)	1.00(1)	**0.350**(5)	0.54(2)	**none**	--	--
REF-550	**20.9**(3)	**1.481**(7)	3.7850(1)	9.5179(2)	0.02(1)	0.41(2)	0.1666(1)	1.00(1)	**0.067**(6)	1.0(1)	**R**	**93.24**(5)	32.3(5)

A. Appropriateness of the microstructural models

Before accepting final LPA results the appropriateness of the microstructural models used in the XRD data modelling is discussed here. To illustrate the broadening effects the WH-plots for three selected samples are depicted in Figures 2(a) and 2(b). There is a huge peak overlap in most cases and hence the line widths could not be extracted directly. It was done *a posteriori*, after the Rietveld refinement – the refined peak parameters were used to simulate the pattern as a sum of pseudo-Voigt peaks. Widths and shape parameters were refined for each reflection independently, whereas the other parameters (positions, intensities) were kept fixed. WH-plots of two samples from the nBUT series are depicted in Figure 2(a). It is evident that the size broadening effect is dominant and that the crystallites size is growing with increasing annealing temperature. Contrary the WH-plot of the ISOP-400 sample in Figure 2(b) shows that the defect induced broadening is nonnegligible and an incautious use of the Scherrer equation (Langford and Wilson, 1978) would be unjustified. Small dispersion of the points around the linear fit in Figures 2(a) and 2(b) shows that *hkl*-anisotropy effects are rather weak.

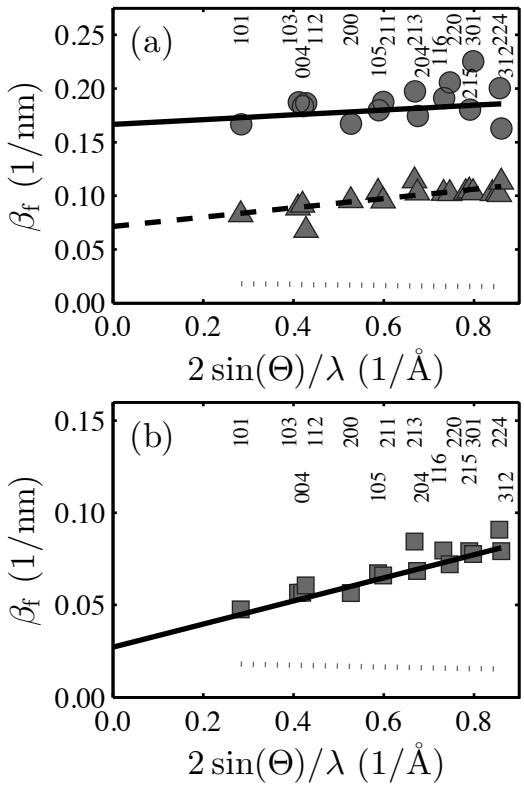

Figure 2. WH-plots for the (a) nBUT-300 (circles), nBUT-450 (triangles) samples and for the (b) ISOP-400 sample (squares). Integral breadths β_f are plotted for different reflections with instrumental broadening already deconvoluted. The instrumental broadening is depicted by a dotted line.

https://doi.org/10.1017/S0885715613001061 Published online by Cambridge University Press

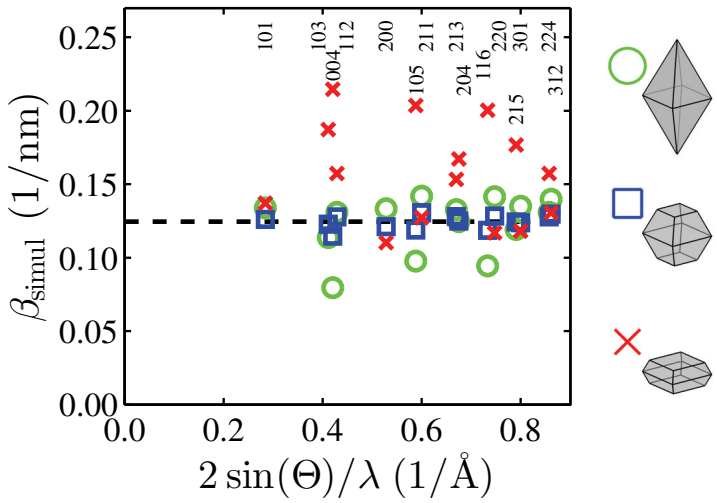

Figure 3. (Color online) WH-plots simulated for the bipyramidal anatase crystallites with different ratio (r) of the dimension in the truncating and the basal plane: r = 0 (green circles), r = 0.58 (blue squares) and r = 0.8 (red crosses). Mean value from the breadths from crystallite with r = 0.58 is depicted by a dashed line.

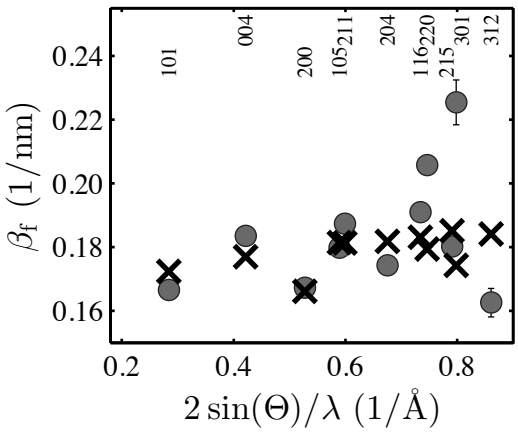

Figure 4. Fit of the WH-plot of the nBUT-300 sample with the truncated bipyramidal crystallites model: selected (these with experimental variations determined) measured (circles) and calculated (crosses) integral breadths.

Figures 3 and 4 should give a more quantitative insight. It is commonly accepted that anatase crystallites have the shape of bipyramids formed by {101} facets. Barnard and Zapol (2004) and Barnard and Curtiss (2005) theoretically studied phase stability and morphology of titania nano-particles and they found that anatase crystallites prefer shape of bypiramids truncated by {001} facets, which proportions can be influenced by e.g. surface hydrogenation or acidic conditions. Anatase crystals of the truncated bipyramidal shape were synthesised by Yang *et al.* (2008). The crystallites were strongly shortened in the *c*-direction having large fraction of the {001} facets but they were about few microns large. In papers of Cernuto *et al.* (2011), Jensen *et al.* (2010)

https://doi.org/10.1017/S0885715613001061 Published online by Cambridge University Press

and Štengl *et al.* (2011) nanocrystallites were on the contrary elongated along the *c*-direction. In order to investigate how such the bipyramidal shape could be exposed in the anisotropy of diffraction line widths, integral breadths for crystallites of such shape were simulated using the method proposed by Scardi and Leoni (2001) and recently generalized by Leonardi *et al.* (2012). The essential model parameter here was r – a relative ratio of the crystallite dimension in the truncating and in the basal plane. If $r = 0$ the crystallite has a shape of the full bipyramid. With increasing r the height of the truncated bipyramide is smaller. For $r = 1$ the size of the truncating {001} facets approaches the size of the pyramid base and the object collapses in two dimensions. Results for $r = 0$, 0.58 and 0.8 are depicted in Figure 3. It is visible that completely different anisotropy is produced if crystallites are only slightly truncated ($r \sim 0$) and when the fraction of {001} facets is high ($r \sim 0.8$). Between this two extremes there is a shape ($r \sim 0.58$), which produces fairly isotropic broadening.

From the integral breadths (β_{hkl}) of the nBUT-300 sample reliable data – these with experimental variations determined – were taken and fitted assuming the truncated bipyramidal shape and a simple microstrain (e) broadening.

$$\beta_{hkl} = \beta_{hkl}^{bipyramide} + 4e \sin\theta / \lambda, \qquad (1)$$

The fit is depicted in Figure 4. The refined shape parameter is $r = 0.63$. The model succeeded quite well in matching the first five reflections, demonstrating that crystallites are slightly larger in the *a*-direction than in the *c*-direction. However, the model failed for the scattered high angle reflections. This is not crucial, because the high-angle data originate from strongly overlapped reflections and can be erroneous. In conclusion, the partial success of the model gives a motivation to include a model of Leonardi *et al.* (2012) in the LPA analysis of TiO_2 nanocrystallites but it validates as well a primary assumption that broadening is close to be *hkl*-isotropic in the case under study and the simplest model of spherical crystallites could be adopted for the analysis.

The discussion is finally complemented here by Figure 5 showing a field emission scanning electron microphotograph of the nBUT-450 sample. Particles in Figure 5 are not strictly

https://doi.org/10.1017/S0885715613001061 Published online by Cambridge University Press

spherical but they do not exhibit any substantive shape anisotropy either. The particles are also of approximately the same size as the values determined from XRD ($\langle D \rangle \approx 11$ nm).

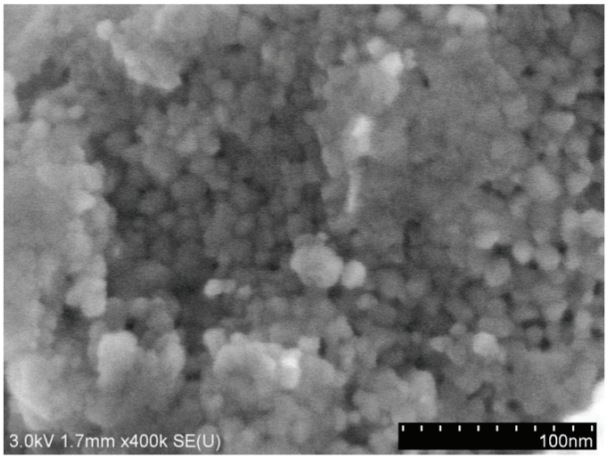

Figure 5. FE-SEM image of the nBUT-450 sample (XRD crystallite size $\langle D \rangle \approx 11$ nm).

B. Microstructure of the synthesised anatase nanoparticles

Microstrain (e) is minor effect for XRD line broadening. It takes values of $e \approx 0.2\% - 0.35\%$ in all the samples, except of ISOP-SubWE/PFE and REF-550. The ISOP-SubWE/PFE sample exhibits the largest microstrain $e \approx 0.8\%$, but in this case the parameter e correlates with temperature factors (B_{iso}) and therefore the parameters can not be determined unambiguously. The lowest microstrain $e \approx 0.07\%$ was found in the REF-550 sample, which was calcined at the highest temperature. This can be explained by a generally accepted presupposition that at higher temperatures crystal defects can be removed more effectively. Nonzero microstrain and dislocation densities in anatase nanoparticles were found also by Vives and Meunier (2009), Weibel *et al.* (2005) or Spadavecchia *et al.* (2010). Djerdj and Tonejc (2006) observed dislocations in anatase directly by TEM.

The first two columns in Table II show the CSD parameters (M and σ^*), which are the most important quantities here from the application point of view. Samples with different crystallites sizes (3—20 nm) were synthesised. CSDs for all the samples are depicted in Figure 6.

https://doi.org/10.1017/S0885715613001061 Published online by Cambridge University Press

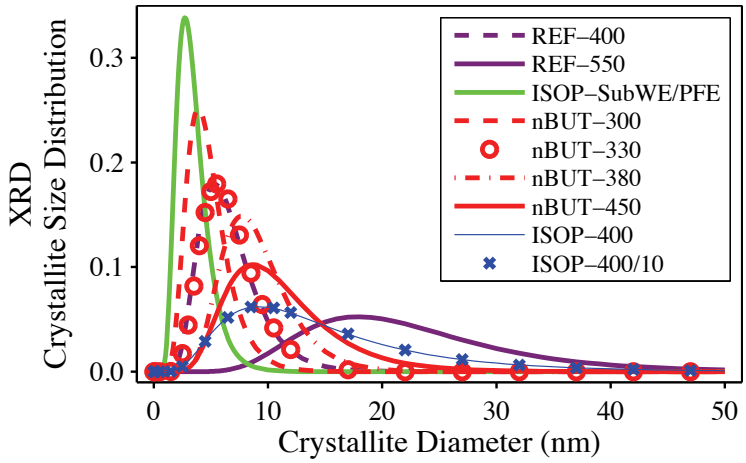

Figure 6. (Color online) Refined CSDs of anatase crystallites plotted for all the samples.

It can be seen that (i) the ISOP-SubWE/PFE sample with the smallest crystallites has a bell shaped CSD. (ii) The same is true for all the nBUT samples, which form a nice series of different crystallite sizes. (iii) Also the ISOP samples REF-400 and REF-550 calcined from the gel at different temperatures have clearly different sizes. Whereas (iv) CSDs of the ISOP samples ISOP-400 and ISOP-400/10 prepared by low-temperature hydrolysis and calcined for different time are indistinguishable. (v) In addition they exhibit larger relative dispersion of crystallite sizes. Their multiplicative standard deviation (σ^*), which determines the variance relative to crystallites size (M), takes the value $\sigma^* \approx 1.8$. For all other samples, it is significantly less, $\sigma^* \approx 1.4$—1.5.

C. Comparison with specific surface area measurements

The powder samples were prepared for applications in catalysis and hence *their specific surface area* was an important parameter. A quantity S_{BET} [BET – Brunauer, Emmett and Teller (Brunauer *et al.*, 1938)] was determined for each sample from nitrogen physisorption experiments [for details see Matějová *et al.* (2010), Matějová *et al.* (2012a), Matějová *et al.* (2012b) or Matěj (2011c)]. From XRD crystallite size a theoretical *total surface area of crystallites* per unit mass (S_{XRD}) can be calculated. It measures crystallites surface from the "inner" side, whereas S_{BET} is related to the surface accessible for a gas from the "outer" side of particles. Despite the fact that these two quantities reflect different features of the material, for instance XRD do not "see" non-crystalline part of the sample, it is quite common to find in the

https://doi.org/10.1017/S0885715613001061 Published online by Cambridge University Press

literature their comparison [e.g. in (Audebrand *et al.*, 2000; Weibel *et al.*, 2005)]. Including contributions from all crystalline phases to S_{XRD}, it follows

$$S_{XRD} = \sum_i \frac{x_i K_i}{\rho_i \langle D \rangle_{i,A}}, \ (\sum_i x_i = 1), \qquad (2)$$

where x_i is the weight fraction of the given phase, ρ_i is its structural density, K_i is the crystallite shape constant ($K = 6$ for sphere) and $\langle D \rangle_{i,A}$ is the area weighted crystallite size, which can be calculated from CSD parameters (M and σ^*).

The comparison of S_{XRD} and S_{BET} values is depicted in Figure 7. They are comparable at least in the order of magnitude for most of the samples with exceptions of the nBUT-450 and REF-550 samples, which were calcined at the highest temperatures. Their $S_{BET} \approx 10$ m^2/g is by an order of size less than $S_{XRD} \approx 50$—100 m^2/g. If S_{BET} is recalculated to sizes it gives $D_{BET} \geq 130$ nm, whereas the XRD sizes are $\langle D \rangle \approx 11$—23 nm. The XRD sizes clearly better correspond with dimensions of primary particles in electron microphotographs (see Figure 5 for the nBUT-450 sample). Such a reduced specific surface area is a typical sign of an agglomeration of crystallites into larger particles (Audebrand *et al.*, 2000). Values for the other samples from the nBUT series are nicely proportional to $1/\langle D \rangle_A$ in Figure 7. In addition, the slope of the linear dependence is very close to the ideal value depicted by a dotted line, which indicates that not much surface is missing. The ISOP-SubWE/PFE sample with the smallest crystallites shows even better agreement between XRD and specific surface. This was attributed in Matějová *et al.* (2012b) to an advantageous effect of methanol in the PFE process. The methanol removes organic contaminants that act as binder between agglomerated crystallites. Another phenomenon is emphasized by a dotted horizontal line in Figure 7. S_{BET} values of samples treated at temperature 400 °C are very similar and are spread in the vicinity of this line. Contrary, the crystallite sizes of these samples differ significantly. In fact the crystallites of ISOP-400 samples are more than 2 times larger than crystallites of REF-400. As they have almost similar S_{BET} this indicates that in the REF-400 sample the porous structure is not as ideal as it could be. The overall discussion here, based on a comparison of data from different series of samples, strengthens conclusions in Matějová *et al.* (2012a). Mainly the annealing temperature, not the crystallites size, affects the specific surface area. These two structural parameters can be correlated at lower annealing temperatures. At the temperatures above 400 °C crystallites tend to agglomerate (Matějová *et al.*, 2012a).

https://doi.org/10.1017/S0885715613001061 Published online by Cambridge University Press

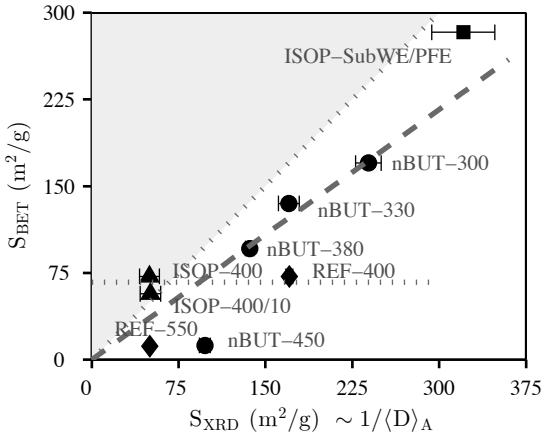

Figure 7. Comparison of measured surface area S_{BET} and theoretical surface area S_{XRD} calculated from XRD CSD parameters.

D. Crystal structure of the synthesised anatase nanoparticles

In this section, the results of samples structure analysis at the atomic scale are presented and their correlation with samples treatment conditions and the microstructural aspects is discussed.

The initial comments concern DW factors, *B*(Ti), *B*(O), and the oxygen atom position *z*(O) in Table II. The values of the DW factors are unusually high, especially in the ISOP-SubWE/PFE sample. As the particular values can be erroneous, e.g. due to parameters correlation during refinement, it is better to follow only trends. Values of *B*(O) are decreasing with growing crystallites dimension for the set of nBUT samples. Djerdj and Tonejc (2006) observed a similar trend and proposed a plausible explanation. They separated the DW factors into a temperature-dependent and a static part and argued that mainly the static DW factor part is enhanced in nanoparticles because of higher disorder (concentration of defects).

The fractional *z*-coordinate of the oxygen atom takes the value $z(O) \approx 0.166$ close to values for nanocrystalline anatase found in (Djerdj and Tonejc, 2006) or reported by Howard *et al.* (1991) also for larger particles. The most distinct value, $z \approx 0.170$, is associated again with the ISOP-SubWE/PFE sample. Systematic dependence of the oxygen *z*-coordinate on crystallites size (but of opposite character) was observed by Swamy *et al.* (2006) in sol-gel anatase nanoparticles.

The strongest correlations were found between two parameters – the samples synthesis temperature and the particles size, and data in three undiscussed columns of Table II – crystal lattice parameters (*a*, *c*) and occupancy of the Ti^{4+} lattice site, *Occ*(Ti). Figure 8(a) depicts a

https://doi.org/10.1017/S0885715613001061 Published online by Cambridge University Press

relation between the Ti-occupancy and crystallites mean size ⟨D⟩. The data are well fitted by the exponential function. It should be noted, that the size dependent Ti-occupancy was observed also by Bokhimi *et al.* (1995), Swamy *et al.* (2006) and Grey and Wilson (2007). They reported the occupancy of about 80% in anatase particles of size 2—4 nm.

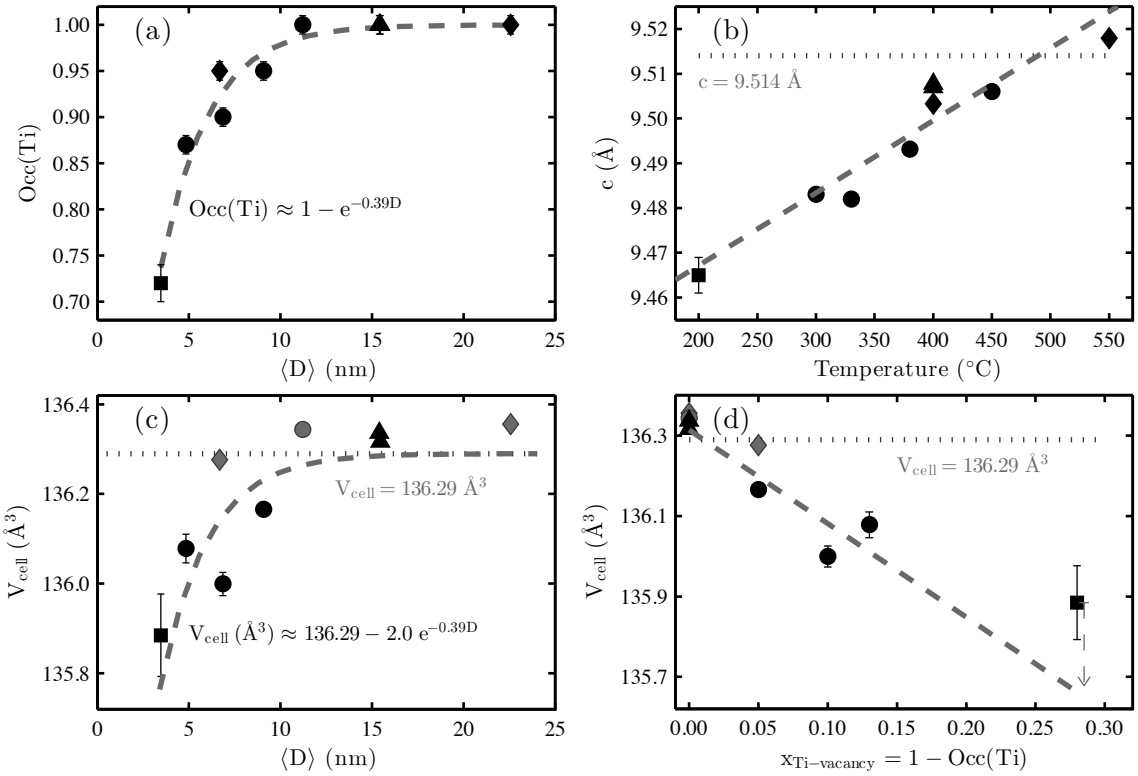

Figure 8. Correlations between various structural parameters (Ti-occupancy, anatase lattice parameter and volume), crystallites size and synthesis temperature. ISOP-SubWe/PFE (square), nBUTs (circles), REFs (diamonds), ISOPs-400 (triangles). Literature bulk data are depicted by shadow dotted lines, fits by dashed lines. Shadow points were omitted from the fitting. An arrow in subplot (d) shows the cell volume correction calculated from Grey and Wilson (2007).

Temperature dependence of the *c*-lattice parameter is depicted in Figure 8(b). The *c*-lattice parameter is close to the value $c = 9.514$ Å reported by Howard *et al.* (1991) in samples treated at the highest temperature and it is strongly contracted at lower synthesis temperatures. The maximum absolute difference is about $\Delta c \approx 0.05$ Å in the size range of $\langle D \rangle = 3.5$—23 nm. By contrast, the lattice *a*-parameter is elongated in the smallest particles and approaches the value $a = 3.7845$ Å (Howard *et al.*, 1991) in samples with the largest particles (Table II). The maximum difference $\Delta a \approx 0.0025$ Å is approximately 20 times smaller than Δc, hence anatase *c*-parameter and the unit cell volume (V_{cell}) follows similar trends. It was mentioned that the crystallite size of studied samples is not a unique function of the final treatment temperature,

https://doi.org/10.1017/S0885715613001061 Published online by Cambridge University Press

hence correlation between the *c*-lattice parameter and crystallites size is not so good, however the trend is preserved. A strong contraction of the *c*-parameter with decreasing crystallites size is in a good agreement with literature (Bokhimi *et al.*, 1995; Djerdj and Tonejc, 2006; Swamy *et al.*, 2006; Grey and Wilson, 2007; Ahmad and Bhattacharya, 2009), but the same is not true for the *a*-parameter. In all the references, the *a*-parameter was much more strongly elongated in very small ($D \leq 10$ nm) crystallites. The anisotropy of the lattice parameters dependence on particles size finally resulted in a V_{cell} expansion with decreasing particles size in such small crystallites and opposite or almost constant behaviour in larger crystallites. This general behaviour was recognised by Luca (2009), who argued that the cell volume expansion for the smallest particle sizes is due to a surface stress in nanoparticles. The V_{cell} dependence on crystallites size of the studied samples is depicted in Figure 8(c). The effect of lattice cell volume contraction with decreasing crystallites size is clearly visible. Only a single point (ISOP-SubWE/PFE) could be considered as a sign of the above effect of Luca (2009). However, monotonic dependence of V_{cell} on crystallites size was also observed by Li *et al.* (2005) and Grey and Wilson (2007). Besides the surface stress effect, there are other theories concerning correlations between the Ti-occupancy, unit cell volume and particles size. Iacomino *et al.* (2008) discussed the influence of surface coverage, Djerdj and Tonejc (2006) proposed a correlation between variation of lattice parameters and dislocation induced lattice strains and Grey and Wilson (2007) studied, by molecular modelling, the stability of Ti-vacancies in anatase nanocrystals and their effect on the unit cell parameters. To investigate this relation in the studied samples, V_{cell} was plotted vs. Ti-vacancy probability $x_{\text{Ti-vacany}} = 1\text{-}Occ(\text{Ti})$ at Ti-sites in Figure 8(d). The interpolation functions in Figure 8(a) and 8(c) are very similar and hence it is straightforward to fit data in Figure 8(d) by a straight line:

$$\Delta V_{\text{cell}} / V_{\text{cell}} = (-0.017 \pm 0.003) \cdot x_{\text{Ti-vacancy}}. \qquad (3)$$

The fit is not optimal, the analysis relies on small deviations from the bulk values and the initial patterns fits (Figure 1) were also not perfect. This could be related to the limits of the Rietveld and WPPM methods used for the analysis. Appropriates of the Rietveld method for similar cases has been already discussed by Grey and Wilson (2007). They used the Debye formula method (Proffen and Neder, 1997) to simulate XRD powder patterns from anatase nanoclusters and analysed the simulated data by conventional Rietveld software. They found that when Ti-vacancies

https://doi.org/10.1017/S0885715613001061 Published online by Cambridge University Press

are distributed homogeneously throughout the nanoparticle the Ritveld method correctly reproduces the vacancies concentration. However, the lattice parameters determined by the Bragg-diffraction-based Rietveld method are strongly overestimated for anatase crystallite sizes below 4 nm. Such an effect would result in effective overestimation of the unit cell volume. The correction was calculated from the data in Grey and Wilson (2007) for the sample with the smallest crystallites ($\langle D \rangle$ = 3.5 nm) and it is depicted in Figure 8(d). The problem discussed above and the surface stress effect of Luca (2009) can influence the cell volume contraction coefficient in Eq. (3). Actually, both effects would lead to underestimation of the absolute value of the coefficient.

V. CONCLUSION

Nanocrystalline anatase powders synthesised by various chemical methods were studied by XRD and the WPPM method in order to reveal cross series correlations within the structural and micro-structural parameters, sample treatment conditions and the application properties. The WPPM was complemented by the WH analysis of diffraction profiles widths. Anisotropy of the diffraction line broadening due to the truncated bipyramidal shape of anatase crystals was discussed. It was shown that such crystallite shape can induce different types of *hkl*-anisotropy in dependence on the relative ratio of the crystallite dimensions. In the extreme cases of the full bipyramidal shape and the case of strongly shortened crystallites in the *c*-direction the anisotropy effects are strong and can be easily detected. Contrary, for a proper ratio of crystallite dimensions the broadening is almost *hkl*-isotropic. This was the case for the studied samples. The size of synthesised anatase nanoparticles varied in the range 3–25 nm in dependence on both, the sample treatment temperature and the synthesis route. The theoretical total surface area of crystallites estimated from XRD parameters was in a good correlation with the surface area measured by the nitrogen physisorption up to the temperature 400–450 °C, when the particles started to agglomerate. Anatase lattice parameters and Ti-site occupancy varied with the synthesis temperature and the crystallites size. Significant (10—30%) deficiency in the Ti-occupancy was detected in small ($D \leq 10$ nm) nanoparticles. It was strongly correlated with crystallites size. In addition, a systematic anatase unit cell volume contraction with decreasing crystallites size was observed and both effects were attributed to the presence of Ti-vacancies. Linear coefficient between the cell volume contraction and Ti-vacancies concentration was estimated.

https://doi.org/10.1017/S0885715613001061 Published online by Cambridge University Press

ACKNOWLEDGMENTS

This work has been supported by the Grant Agency of the Czech Republic (project P108/11/1539) and within the Charles University Research Center "Physics of Condensed Matter and Functional Materials" (UNCE 204023/2012). The authors are also very grateful to Mr. Jiří Franc (in memoriam) from J. Heyrovsky Institute of Physical Chemistry of the ASCR, v.v.i. for providing the FE-SEM images.

Ahmad, M. I. and Bhattacharya, S. S. (**2009**). "Size effect on the lattice parameters of nanocrystalline anatase," Appl. Phys. Lett. **95**, 191906.

Arlt, T., Bermejo, M., Blanco, M. A., Gerward, L., Jianq, J., Olsen, J. S. and Recio, J. M. (**2000**). "High-pressure polymorphs of anatase TiO_2," Phys. Rev. B: Solid State **61**, 14414–14419.

Audebrand, N., Auffrédic, J.-P. and Louër, D. (**2000**). "An X-ray powder diffraction study of the microstructure and growth kinetics of nanoscale crystallites obtained from hydrated cerium oxides," Chem. Mater. **12**, 1791–1799.

Barnard, A. S. and Zapol, P. (**2004**). "Predicting the energetics, phase stability,and morphology evolution of faceted and spherical anatase nanocrystals," Phys. Rev. B: Solid State **108**, 18435–18440.

Barnard, A. S. and Curtiss, L. A. (**2005**). "Prediction of TiO_2 nanoparticle phase and shape transitions controlled by surface chemistry," Nano Lett. **5**, 1261–1266.

Beyerlein, K. R., Snyder, R. L. and Scardi, P. (**2011**). "Powder diffraction line profiles from the size and shape of nanocrystallites," J. Appl. Crystallogr. **44**, 945–953.

Bokhimi, X., Morales, A., Novaro, O., Lopez, T., Sanchez, E. and Gomez, R. (**1995**). "Effect of hydrolysis catalyst on the Ti deficiency and crystallite size of sol-gel-TiO_2 crystalline phases," J. Mater. Res. **10**, 2788–2796.

Bontempi, E., Zanola, P., Gelfi, M., Zucca, M., Depero, L.E., Girault, B., Goudeau, P., Geandier, G., Bourhis, E.L. and Renault, P.-O. (**2010**). "Elastic behaviour of titanium dioxide films on polyimide substrates studied by in situ tensile testing in a X-ray diffractometer," Nucl. Instrum. Methods Phys. Res., Sect. B **268**, 365–369.

Borgese, L., Bontempi, E., Gelfi, M., Depero, L.E., Goudeau, P., Geandier, G. and Thiaudière, D. (**2011**). "Microstructure and elastic properties of atomic layer deposited TiO_2 anatase thin films," Acta Mater. **59**, 2891–2900.

Brunauer, S., Emmett, P. H. and Teller, E. (**1938**). "Adsorption of gases in multimolecular layers," J. Am. Chem. Soc. **60**, 309–319.

Cernuto, G., Masciocchi, N., Cervellino, A., Colonna, G. M. and Guagliardi, A. (**2011**). "Size and shape dependence of the photocatalytic activity of TiO_2 nanocrystals: A total scattering Debye function study," J. Am. Chem. Soc. **133**, 3114–3119.

Djerdj, I. and Tonejc, A. (**2006**). "Structural investigations of nanocrystalline TiO_2 samples," J. Alloys Compd. **413**, 159–174.

Favre-Nicolin, V. and Černý, R. (**2002**). "FOX, 'free objects for crystallography': a modular approach to ab initio structure determination from powder diffraction," J. Appl. Crystallogr. **35**, 734–743.

Fujishima, A. and Zhang, X. (**2006**). "Titanium dioxide photocatalysis: present situation and future approaches," C. R. Chim. **9**, 750–760.

Grey, I. and Wilson, N. C. (**2007**). "Titanium vacancy defects in sol–gel prepared anatase," J. Solid State. Chem. **180**, 670–678.

Hanaor, D. A. H. and Sorrell, C. C. (**2011**). "Review of the anatase to rutile phase transformation," J. Mater. Sci. **46**, 855–874.

Hashimoto, K., Irie, H. and Fujishima, A. (**2005**). "TiO_2 photocatalysis: A historical overview and future prospects," Jpn. J. Appl. Phys. **44**, 8269–8285.

Howard, C. J., Sabine, T. M. and Dickson, F. (**1991**). "Structural and thermal parameters for rutile and anatase," Acta Crystallogr., Sect. B: Struct. Sci. **47**, 462–468.

Chen, B., Zhang, H., Dunphy-Guzman, K. A., Spagnoli, D., Kruger, M. B., Muthu, D., Kunz, M., Fakra, S. and Hu, J. (**2009**). "Size-dependent elasticity of nanocrystalline titania," Phys. Rev. B: Solid State **79**, 125406.

Iacomino, A., Cantele, G., Ninno, D., Marri, I. and Ossicini, S. (**2008**). "Structural, electronic and surface properties of anatase TiO_2 nanocrystals from first principles," Phys. Rev. B: Solid State **78**, 075405.

Jensen, G. V., Bremholm, M., Lock, N., Deen, G. R., Jensen, T. R., Iversen, B. B., Niederberger, M., Pedersen, J. S. and Birkedal, H. (**2010**). "Anisotropic crystal growth kinetics of anatase TiO_2 nanoparticles synthesized in a nonaqueous medium," Chem. Mater. **22**, 6044–6055.

Kužel, R., Nichtová, L., Matěj, Z. and Musil, J. (**2010**). "In-situ X-ray diffraction studies of time and thickness dependence of crystallization of amorphous TiO_2 thin films and stress evolution," Thin Solid Films **519**, 1649–1654.

Langford, J. I. and Wilson, A. J. C. (**1978**). "Scherrer after sixty years: A survey and some new results in the determination of crystallite size," J. Appl. Crystallogr. **11**, 102–113.

Langford, J. I., Louër, D. and Scardi, P. (**2000**). "Effect of a crystallite size distribution on X-ray diffraction line profiles and whole-powder-pattern fitting," J. Appl. Crystallogr. **33**, 964–974.

Leonardi, A., Leoni, M., Siboni, S. and Scardi, P. (**2012**). "Common volume functions and diffraction line profiles of polyhedral domains," J. Appl. Crystallogr. **45**, 1162–1172.

https://doi.org/10.1017/S0885715613001061 Published online by Cambridge University Press

Leoni, M., Martinez-Garcia, J. and Scardi, P. (**2007**). "Dislocation effects in powder diffraction," J. Appl. Crystallogr. **40**, 719–724.

Li, G., Li, L., Boerio-Goates, J. and Woodfield, B. F. (**2005**). "High purity anatase TiO_2 nanocrystals: Near room-temperature synthesis, grain growth kinetics and surface hydration chemistry," J. Am. Chem. Soc. **127**, 8659–8666.

Li, Y.-F. and Liu, Z.-P. (**2011**). "Particle size, shape and activity for photocatalysis on titania anatase nanoparticles in aqueous surroundings," J. Am. Chem. Soc. **133**, 15743–15752.

Limpert, E., Stahel, W. A. and Abbt, M. (**2001**). "Log-normal distributions across the sciences: Keys and clues," BioScience **51**, 341–352.

Luca, V. (**2009**). "Comparison of size-dependent structural and electronic properties of anatase and rutile nanoparticles," J. Phys. Chem. C **113**, 6367–6380.

Matějová, L., Cajthaml, T., Matěj, Z., Benada, O., Klusoň, P. and Šolcová, O. (**2010**). "Super/subcritical fluid extractions for preparation of the crystalline titania," J. Supercrit. Fluids **52**, 215–221.

Matějová, L., Matěj, Z. and Šolcová, O. (**2012**). "A facile synthesis of well-defined titania nanocrystallites: Study on their growth, morphology and surface properties," Microporous Mesoporous Mater. **154**, 187–195.

Matějová, L., Matěj, Z., Fajgar, R., Cajthaml, T. and Šolcová, O. (**2012**). "TiO_2 powders synthesized by pressurized fluid extraction and supercritical drying: Effect of water and methanol on structural properties and purity," Mater. Res. Bull. **47**, 3573–3579.

Matěj, Z. and Kužel, R. (**2009**). MStruct - program/library for MicroStructure analysis by powder diffraction. <http://www.xray.cz/mstruct/> (July 7, 2013).

Matěj, Z., Kužel, R. and Nichtová, L. (**2010**). "XRD total pattern fitting applied to study of microstructure of TiO_2 films," Powder. Diffr. **25**, 125–131.

Matěj, Z., Matějová, L., Novotný, F., Drahokoupil, J. and Kužel, R. (**2011**). "Determination of crystallite size distribution histogram in nanocrystalline anatase powders by XRD," Z. Kristallogr. Proc. **1**, 87–92.

Matěj, Z., Kužel, R. and Nichtová, L. (**2011**). "X-Ray diffraction analysis of residual stress in thin polycrystalline anatase films and elastic anisotropy of anatase," Metall. Mater. Trans. A **42**, 3323–3332.

Matěj, Z. (**2011**). "Structure of submicrocrystalline materials studied by X-ray diffraction," PhD thesis, Charles University in Prague, Faculty of Mathematics and Physics; sec. 4.4.4.

Mills, A., Hill, G., Bhopal, S., Parkin, I. P. and O'Neill, S. A. (**2003**). "Thick titanium dioxide films for semiconductor photocatalysis," J. Photochem. Photobiol., A **160**, 185–194.

https://doi.org/10.1017/S0885715613001061 Published online by Cambridge University Press

Popa, N. C. (**1998**). “The (hkl) dependence of diffraction-line broadening caused by strain and size for all Laue groups in Rietveld refinement,” J. Appl. Crystallogr. **31**, 176–180.

Proffen, T. and Neder, R. B. (**1997**). “DISCUS: a program for diffuse scattering and defect-structure simulation,” J. Appl. Crystallogr. **30**, 171–175.

Sakai, N., Fujishima, A., Watanabe, T. and Hashimoto, K. (**2003**). “Quantitative evaluation of the photoinduced hydrophilic conversion properties of TiO_2 thin film surfaces by the reciprocal of contact angle,” Phys. Rev. B: Solid State **107**, 1028–1035.

Scardi, P. and Leoni, M. (**2001**). “Diffraction line profiles from polydisperse crystalline systems,” Acta Crystallogr., Sect. A: Found. Crystallogr. **57**, 604–613.

Scardi, P. and Leoni, M. (**2002**). “Whole powder pattern modelling,” Acta Crystallogr., Sect. A: Found. Crystallogr. **58**, 190–200.

Spadavecchia, F., Cappelletti, G., Ardizzone, S., Bianchi, C. L., Cappelli, S., Oliva, C., Scardi, P., Leoni, M. and Fermo. P. (**2010**). “Solar photoactivity of nano-N-TiO_2 from tertiary amine: role of defects and paramagnetic species,” Appl. Catal. B **96**, 314–322.

Stephens, P. W. (**1999**). “Phenomenological model of anisotropic peak broadening in powder diffraction,” J. Appl. Crystallogr. **32**, 281–289.

Swamy, V., Menzies, D., Muddle, B. C., Kuznetsov, A. and Dubrovinsky, L. S. (**2006**). “Nonlinear size dependence of anatase TiO_2 lattice parametes,” Appl. Phys. Lett. **88**, 243103.

Štengl, V., Velická, J., Maříková, M. and Grygar, T. M. (**2011**). “New generation photocatalysts: How tungsten influences the nanostructure and photocatalytic activity of TiO_2 in the UV and visible regions,” ACS Appl. Mater. Interfaces **3**, 4014–4023.

Vives, S. and Meunier, C**.** (**2009**). “Influence of the X-ray diffraction line profile analysis method on the structural and microstructural parameters determination of sol-gel TiO_2 powders,” Powder Diffr. **24**, 205–220.

Wang, Y.-Q., Chen, S.-G., Tang, X.-H., Palchik, O., Zaban, A., Koltypin, Y. and Gedanken, A. (**2001**). “Mesoporous titanium dioxide: sonochemical synthesis and application in dye-sensitized solar cells,” J. Mater. Chem. **11**, 521–526.

Weibel, A., Bouchet, R., Boulc', F. and Knauth, P. (**2005**). “The big problem of small particles: A comparison of methods for determination of particle size in nanocrystalline anatase powders,” Chem. Mater. **17**, 2378–2385.

Yang, H. G., Sun, C. H., Qiao, S. Z., Zou, J., Liu, G., Smith, S. C., Cheng, H. M. and Lu, G. Q. (**2008**). “Anatase TiO_2 single crystals with a large percentage of reactive facets,” Nature **453**, 638–641.

Zhang, H. and Banfield, J. F. (**1998**). “Thermodynamic analysis of phase stability of nanocrystalline titania,” J. Mater. Chem. **8**, 2073–2076.

https://doi.org/10.1017/S0885715613001061 Published online by Cambridge University Press

Zhang, H. and Banfield, J. F. (**2002**). "Kinetics of crystallization and crystal growth of nanocrystalline anatase in nanometer-sized amorphous titania," Chem. Mater. **14**, 4145–4154.

Zhang, H., Chen, B., Banfield, J. F. and Waychunas, G. A. (**2008**). "Atomic structure of nanometer-sized amorphous TiO_2," Phys. Rev. B: Solid State **78**, 214106.

https://doi.org/10.1017/S0885715613001061 Published online by Cambridge University Press